# Target classification using radar cross-section statistics of millimeter-wave scattering

Aysu Coşkun and Sándor Bilicz
*Department of Broadband Infocommunications and Electromagnetic Theory, Faculty of Electrical Engineering and Informatics, Budapest University of Technology and Economics, Budapest, Hungary*

Received 29 December 2022
Revised 28 April 2023
Accepted 7 June 2023

## Abstract

**Purpose** – This paper aims to discuss the classification of targets based on their radar cross-section (RCS). The wavelength, the dimensions of the targets and the distance from the antenna are in the order of 1 mm, 1 m and 10 m, respectively.

**Design/methodology/approach** – The near-field RCS is considered, and the physical optics approximation is used for its numerical calculation. To model real scenarios, the authors assume that the incident angle is a random variable within a narrow interval, and repeated observations of the RCS are made for its random realizations. Then, the histogram of the RCS is calculated from the samples. The authors use a nearest neighbor rule to classify conducting plates with different shapes based on their RCS histogram.

**Findings** – This setup is considered as a simple model of traffic road sign classification by millimeter-wavelength radar. The performance and limitations of the algorithm are demonstrated through a set of representative numerical examples.

**Originality/value** – The proposed method extends the existing tools by using near-field RCS histograms as target features to achieve a classification algorithm.

**Keywords** Classification, Histogram, Machine learning, Radar cross-section, Physical optics

**Paper type** Research paper

## 1. Introduction

Radars operating in the millimeter-wavelength (mmWave) band are more and more widespread, e.g. in driving assistance systems (DAS) (Kosuge *et al.*, 2022). The numerical simulation of mmWave radar operation is still challenging, both in terms of electromagnetic wave scattering and prediction of the detection/classification capabilities of the system as well.

Targets of interest in DAS (e.g. vehicles, pedestrians, traffic road signs) are much larger than the wavelength. Therefore, asymptotic approximations [e.g. physical optics (PO)] are the only reasonable choice for the simulation of EM scattering. Furthermore, the scattered field is very sensitive to small angular variations of the target's orientation. In addition to that, targets are typically in the near field of the radar's antenna; thus, the classical definition



This research is supported by the Hungarian Scientific Research Fund under Grant K-135307.

COMPEL - The international journal for computation and mathematics in electrical and electronic engineering
Vol. 42 No. 5, 2023
pp. 1199-1211
Emerald Publishing Limited
0332-1649
DOI 10.1108/COMPEL-12-2022-0446

of radar cross-section (RCS) needs to be extended, by introducing the near-field RCS (Pouliguen *et al.*, 2006; Elfrgani and Reddy, 2019).

The target detection and classification task of mmWave DAS radars are intensively studied. Many approaches strongly rely on the particular signal processing architecture, especially frequency-modulated continuous wave (FMCW) radars, e.g. Kim *et al.* (2022). Obviously, deep learning is also proposed for target classification: range-azimuth distributions of the power of the radar echo are considered as image data, which feed deep neural networks to predict some attributes of the target (Patel *et al.*, 2019). This approach is efficiently combined with an FMCW architecture in (Gupta *et al.*, 2021), and excellent classification accuracy is reached.

Other approaches consider the statistical properties of the RCS. When observations are repeated within a certain (small) time interval, variations in the scenario (e.g. rotation or vibration of the target) induce the change of the RCS, too. As the scenario varies in an uncontrollable and unknown manner, the RCS is modeled as a random variable. It has been shown decades ago that the probability density function (approximated by the histogram) of the RCS characterizes the target's properties; this is the key idea behind the Swerling models (Swerling, 1960). Recently, the histogram of the RCS was again proposed for classification (Vladyslav and Maxim, 2016) and for enhancing the capabilities of air surveillance radars (Vaila *et al.*, 2017). Statistical description of the RCS is combined with cutting-edge learning methods to classify targets in the thorough work (Cai *et al.*, 2021) with which our approaches have a lot in common, yet they apply parametric distributions to describe the RCS, whereas we use histograms as non-parametric RCS descriptions.

In the present work, we consider a simple model for traffic road sign classification based on mmWave radar observations. Our contribution is twofold:

(1) we study the near-field RCS and its histogram for simple objects by means of PO simulations; and

(2) we apply a supervised learning method [$K$-nearest neighbor (KNN) rule] for the shape classification of traffic road signs based on their RCS histogram.

## 2. Radar cross-section (RCS) and its calculation

### *2.1 Radar cross-section in the far- and near-field*

RCS is classically defined as:

$$\sigma_0 = \lim_{R\to\infty} 4\pi R^2 \frac{S_r}{S_i}, \tag{1}$$

where $S_i$ is the incident power density at the target, $S_r$ are the reflected power density at the antenna and $R$ is the distance between the antenna and the target. As $S_r$ is proportional to $R^{-2}$, the limit yields a finite value of $\sigma_0$, which does not depend on $R$ (Skolnik, 1990). As long as the target is in the far field (Fraunhofer region) of the antenna, the power of the echo received by the antenna is proportional to $\sigma_0$. The far field is commonly defined as:

$$R > R_F = \frac{2D^2}{\lambda}, \tag{2}$$

where $R$ is the distance from the antenna, and the limit $R_F$ is calculated from the diameter of the target $D$ (or the aperture of the antenna, if it is larger), and the wavelength $\lambda$.

However, in the case of mmWave radar, Condition (2) is not met. For example, in a driving assistance system operating at 77 GHz ($\lambda \approx 4$ mm), $D$ is in the order of 1 m; hence, $R_F \approx 500$ m, which is much larger than the range of interest of the radar. Therefore, the RCS definition (1) cannot be applied in such scenarios, but herein we will use the formula:

$$\sigma = 4\pi R^2 \frac{S_r}{S_i}, \tag{3}$$

yielding the near-field RCS $\sigma$ that depends on $R$, as concluded also in Taylor and Terzuoli (1997).

*2.2 Simulation by the physical optics (PO) approximation*

In this work, we consider targets made of a good conductor, having a linear extent much larger than the wavelength. Therefore, the RCS [as given in equation (3)] is numerically calculated by means of the PO approximation. This method has been applied for decades (Kouyoumjian, 1965; Bowman *et al.*, 1969). The key assumption of PO is that the surface current generated on a conducting body is approximated as:

$$\mathbf{J}_S = \begin{cases} 2\hat{\mathbf{n}} \times \mathbf{H}^i, & \text{on the illuminated surface,} \\ 0, & \text{on the shadowed surface,} \end{cases} \tag{4}$$

where $\hat{\mathbf{n}}$ is the outward normal vector of the surface, and $\mathbf{H}^i$ is the magnetic field strength in the incident field. Let us consider the configuration sketched in Figure 1, and assume that an infinitesimal dipole antenna is placed at the position $\boldsymbol{r}$. This antenna transmits the EM wave and receives the echo, i.e. a monostatic configuration is considered. For the RCS in equation (3), under the assumption (4), one can derive the formula:

$$\sigma = \frac{4\pi}{\lambda^2}\left|\int_\Gamma \cos\alpha(\mathbf{r},\mathbf{r}')\exp\left(-2\mathrm{j}k\rho(\mathbf{r},\mathbf{r}')\right)\mathrm{d}\Gamma'\right|^2, \tag{5}$$

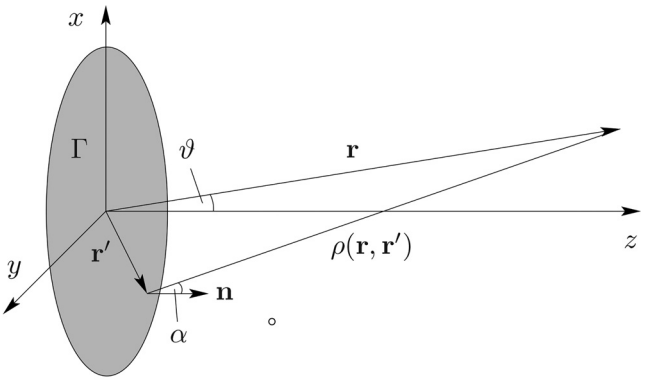


**Notes:** The antenna is at the point ***r***, and the target is represented by the surface Γ

**Source:** Authors' own work

**Figure 1.**
Configuration for calculating the RCS

where $k = 2\pi/\lambda$ stands for the wavenumber, and $\rho$ is the distance between the dipole at $\boldsymbol{r}$ and the point on the target $\mathbf{r}'$. The angle $\alpha$ is the incident angle at the point $\mathbf{r}'$, i.e. $\cos\alpha = \hat{\mathbf{n}}(\mathbf{r} - \mathbf{r}')/\rho$. The integral (5) is numerically evaluated by an in-house Matlab function throughout the examples in this work.

As an illustration, for a circular plate, the near-field RCS calculated by equation (5) is compared to the far-field RCS in Figure 2(a). The frequency equals to 77 GHz. Also, the surface current distribution is plotted in Figure 2(b).

## 3. Histogram-based target classification

### *3.1 Histogram representation of the radar cross-section*

In Figure 2(a), it can also be observed that the RCS strongly fluctuates even when $\vartheta$ has a small variation. As $\vartheta$ can hardly be kept constant in a real-life scenario (e.g. due to the wind, vibration of the car on which the radar is mounted, etc.), we model the radar measurement as follows:

- The parameter $\vartheta$ is defined as a random variable; thus, the RCS is also random.
- Observations are made repeatedly during a short time interval, in which all parameters of the scenario are unchanged, except for $\vartheta$, which takes $n$ random realizations, $\vartheta_i$, $i = 1, 2, \ldots, n$.
- For each $\vartheta_i$, the RCS is calculated by equation (5).
- A histogram is calculated from the samples of the RCS. This histogram is considered as a *feature*, on which the classification is based later on. In Figure 3, it can be observed that histograms indeed strongly depend on the shape and the distance of the target.

To formally define the histogram, let us assign *bins* as:

$$x_1 < x_2 < \ldots < x_b. \tag{6}$$

Herein we use an equal bin width $\Delta x$; thus:

$$x_k = (k-1)\Delta x + x_1, \quad k = 2, 3, \ldots, b. \tag{7}$$

Then the histogram of $n$ random samples is denoted by the vector:

$$\mathbf{h} = [h_0, h_1, h_2, \ldots, h_b], \tag{8}$$

where each element of the vector equals to the number of samples within the related bin, i.e.:

$$h_k = \frac{\#\text{ sample values in the range } [x_k, x_{k+1})}{n}. \tag{9}$$

For $k = 0$ and $k = b$, the lower and upper bound of the interval is extended to $-\infty$ and $+\infty$, respectively.

### *3.2 Classification algorithm*

The classification methodology can be summarized as follows, with the illustration shown in Figure 4. $Q$ number of classes are defined; one class for each shape of the targets. $P$ number of training histograms are generated for each shape. Each training histogram is generated at a different distance from the radar: $R = R_1, R_2, \ldots, R_P$.

We apply the classical $K$-NN algorithm (Devroye *et al.*, 1996) for the classification. We chose this algorithm because we are aiming at the validation of the use of histograms as target features, and this can basically be evaluated even with this simple algorithm. Furthermore, the

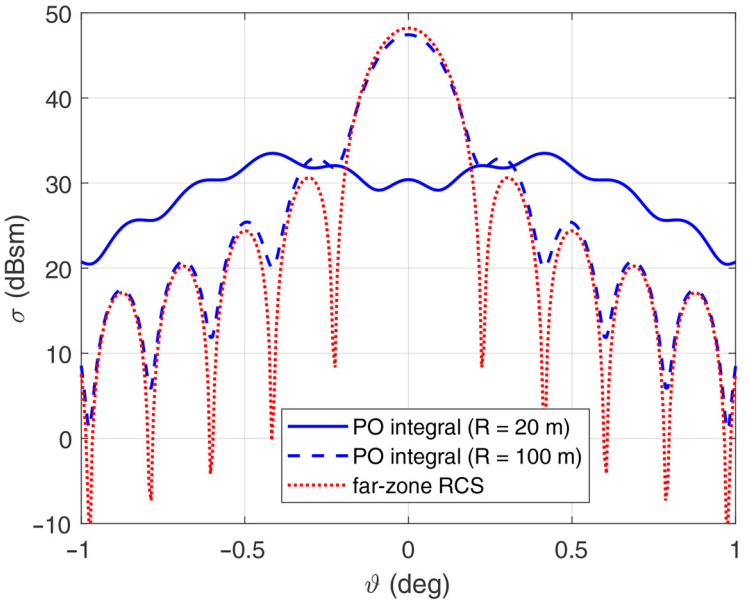


**(a)**

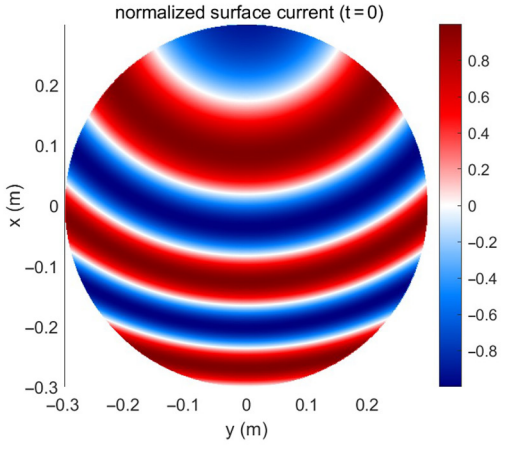


**(b)**

**Notes:** (a) RCS with respect to the incident angle ("dBsm" stands for decibel square meter); (b) Surface current density (instantaneous value, normalized by its maximum), for $\vartheta = 1°$ and $R = 20$ m
**Source:** Authors' own work

**Figure 2.**
A circular plate centered to the origin, perpendicular to $z$, whereas the antenna is at the point $\mathbf{r} = (R \sin \vartheta, 0, R \cos \vartheta$, according to Figure 1

simplicity of the $K$-NN method lets us focus on this main question. The $K$-NN algorithm is summarized as follows. The distance between the histogram to be classified (i.e. the testing histogram), and each $PQ$ histogram within the training sets is calculated. The $K$ number of closest training histograms (i.e. the nearest neighbors) are selected, and a majority voting is held

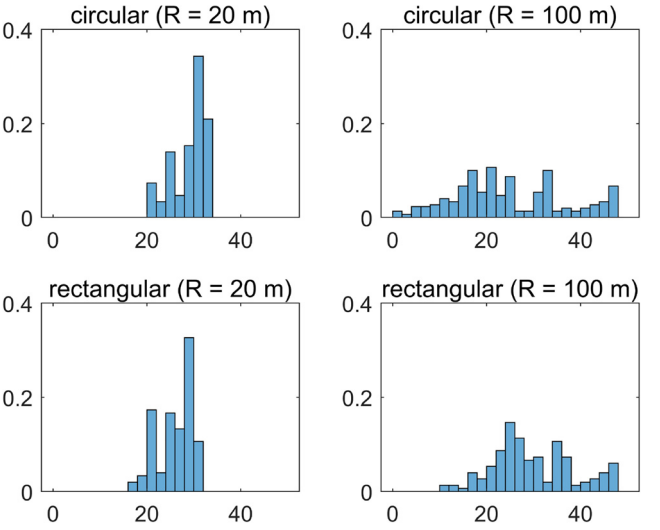


**Figure 3.**
Histograms of the RCS of circular and rectangular plates at different $R$ distances. *Horizontal* axes: $\sigma$ (in dBsm), *vertical* axes: empirical probability density

**Source:** Authors' own work

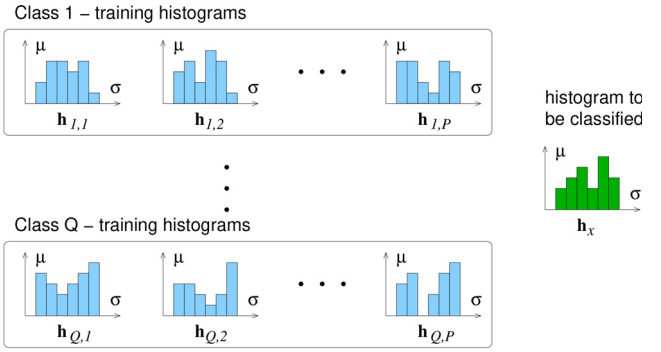


**Figure 4.**
P number of training histograms are present within each of the $Q$ classes

**Note:** The goal is to classify the histogram $\mathbf{h}_x$ into one of the $Q$ classes

**Source:** Authors' own work.

among them, to decide which class the testing histogram will be classified into. The votes are weighted by factors related to the distance, as proposed in the classical work Dudani (1976).

The distance between histograms $\mathbf{h}^{(1)}$ and $\mathbf{h}^{(2)}$ is defined as the L1 norm of their difference (Devroye *et al.*, 1996), which reads as:

$$d\left(\mathbf{h}^{(1)}, \mathbf{h}^{(2)}\right) \triangleq \left|\left|\mathbf{h}^{(1)} - \mathbf{h}^{(2)}\right|\right|_1 = \sum_{k=0}^{b} \left|h_k^{(1)} - h_k^{(2)}\right|. \tag{10}$$

The classification performance is measured by the error rate, which is the number of incorrect classifications over the total number of testing histograms.

*3.3 Model of the noise*

An important part of our work is to study the effect of the measurement uncertainties on the classification performance. To this end, a simple noise model is introduced. Additive white Gaussian noise (AWGN) is applied on the simulated RCS data when generating the testing histograms. The Gaussian distribution is commonly used for modeling random effects; herein our main goal is to test the robustness of the classification algorithm; this is why, AWGN was chosen. In case when proper knowledge on the noise distribution is available, it is straightforward to extend the approach below to another noise model. Formally, the noise-free RCS result from equation (5) is changed as:

$$\tilde{\sigma}_i = \sigma_i + z_i, \quad i = 1, 2, \ldots, n, \tag{11}$$

where $z_i$ is a realization of the zero-mean Gaussian random variable $Z \in \mathcal{N}(0, \mathrm{STD})$, for each repeated observation. STD stands for the standard deviation of the noise, which takes different values in our examples as shown below. Then, the testing histogram is calculated from the noisy samples $\tilde{\sigma}_i$.

## 4. Examples

Numerical examples are presented herein to illustrate the method and demonstrate its performance. The parameters that are common for all studies are as follows:

- Frequency: $f = 77$ GHz, which corresponds to a wavelength of $\lambda = 3.9$ mm.
- The targets are flat plates made of perfect conductor, oriented as shown in Figure 1. Their shape differs (circular, square, triangular), but their area is the same (0.28 $m^2$, which corresponds to a circle with diameter of 0.6 m).
- The incident angle is a random variable with uniform distribution within the interval $[-1, 1]^{\circ}$.
- Bins for the histograms are set as $x_1 = 0$ dBsm, $x_{25} = 50$ dBsm, and the bin width is $\Delta x = 2$ dBsm, respectively. Hence, the histograms are 26-element vectors.
- The number of repeated observations for the histogram generation is $n = 300$ in all cases.

Four different scenarios are presented in the following.

*4.1 Training and testing with histograms at fixed distance*

In the first scenario, $Q = 2$ classes are defined (circle and square plate), and each of them is trained with $P = 1$ histogram that is generated at a distance of $R = 100$ m. The testing histogram comes from the RCS of either a circle or a square plate at the same distance. Let us note that herein only $K = 1$ makes sense in the $K$-NN algorithm. In the noise-free case, the error rate is obviously zero. However, we test the robustness of the classification by increasing the standard deviation (STD) of the noise according to equation (11). For all values of the STD, 200 testing histograms (100 circle and 100 square) are generated, and the error rate is calculated. The error rate vs noise STD is plotted in Figure 5. For instance, the case when the STD is set to 8 dBsm, the classification performs with 10% error rate, or equivalently, 90% of accuracy.

*4.2 Training and testing histograms at varying distance*

In this part, we stress that the near-field RCS does depend on the distance $R$, and we present how this influences the classification performance. Two sub-cases are considered:

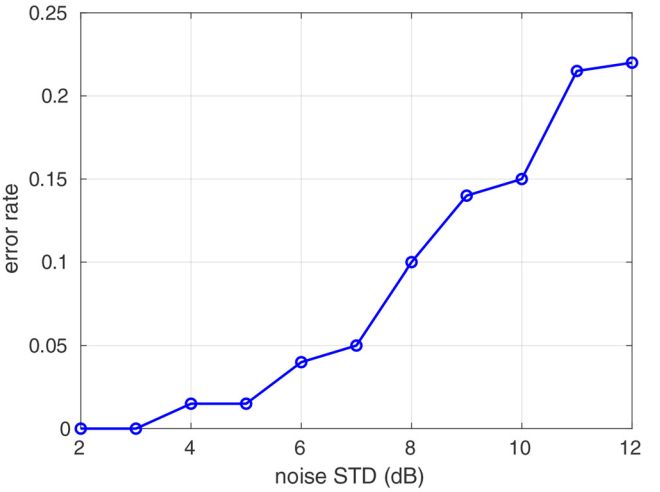


**Figure 5.**
Error rate vs noise STD in the first scenario

**Source:** Authors' own work

(1) First, the training is performed exactly as in the previous part (Section 4a). However, the testing histograms are generated at varying distances, with $R \in [10, 100]$m, in 100 equal steps. No noise is applied now. The results of the classification are shown in Figure 6. When the target is a square plate, the classification is correct at all distances, whereas it fails when the target is a circular plate, being closer to the radar than $\sim 55$ m. This shows that the training set is insufficient in this case.

(2) Second, to overcome the difficulty found in the previous case, we extend the training set by near-field histograms. More precisely, both training classes include $P = 50$ training histograms, generated at distances in the range $R \in [10, 100]$m in 50 equal steps. For testing, 100 circular and 100 square plates are considered, at distances randomly distributed within the same interval as for training. The results for different $K$ values in the $K$-NN algorithm are presented in Figure 7. The accuracy is very high, and interestingly, $K$ seems to have little effect on the performance.

To conclude these two sub-cases, it is seen that the classification algorithm provides a much better performance once relevant data are used for training, with respect to the targets to be classified.

*4.3 Complex targets*

Herein we show examples when complex targets are considered. A complex target is a combination of two plates of simple shape. This can roughly model the case when two traffic road signs are mounted on the same pole. In particular, we consider three targets: "Triangle+Circle," "Circle+Rectangle" and "Triangle+Rectangle," as illustrated in Figure 8. Therefore, the number of classes is $Q = 3$, and for each, $P = 50$ training histograms are generated, with $R \in [10, 100]$m, in $P$ equal steps. For testing, 100 histograms are generated for each type of target, at distances randomly distributed within the same interval as for training. Furthermore, noise is added to the testing data according to equation (11).

The classification performance is presented with different noise STD values, in function of $K$ in Figure 9. Again, it is found that $K$ has little effect on the performance. For low-noise STD, it seems that increasing $K$ lowers the accuracy, whereas this is the opposite for high-noise STD.

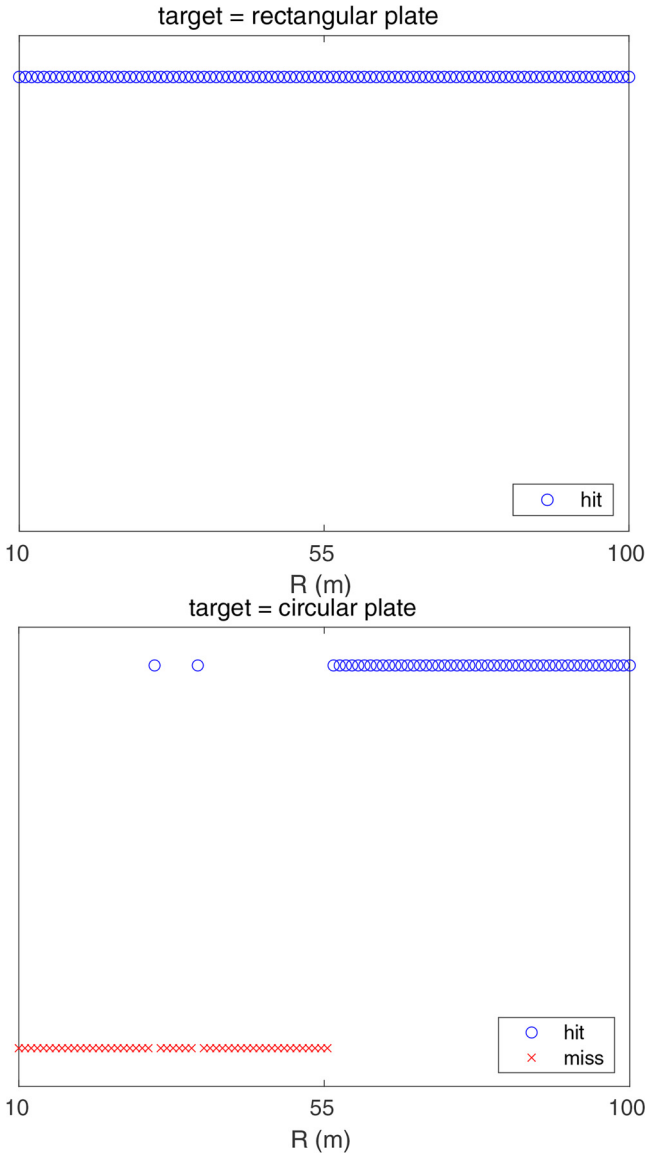


**Source:** Authors' own work

**Figure 6.** Correct (hit) and incorrect (miss) classification vs target distance in the second scenario, when training is made with targets at a fixed distance of $R = 100$ m

Nevertheless, it can also be observed that the error rate about 10% can be achieved only when the noise STD is as low as cca. 0.5 dBsm. Note that in the first scenario (which was much simpler), a significantly higher noise is allowed to obtain similar performance (see Figure 5).

A confusion matrix for $K = 5$ and 1 dBsm of noise STD is presented in Figure 10. Here, the diagonal shows the ratio of correctly classified targets (in percentage). For instance, 91% of

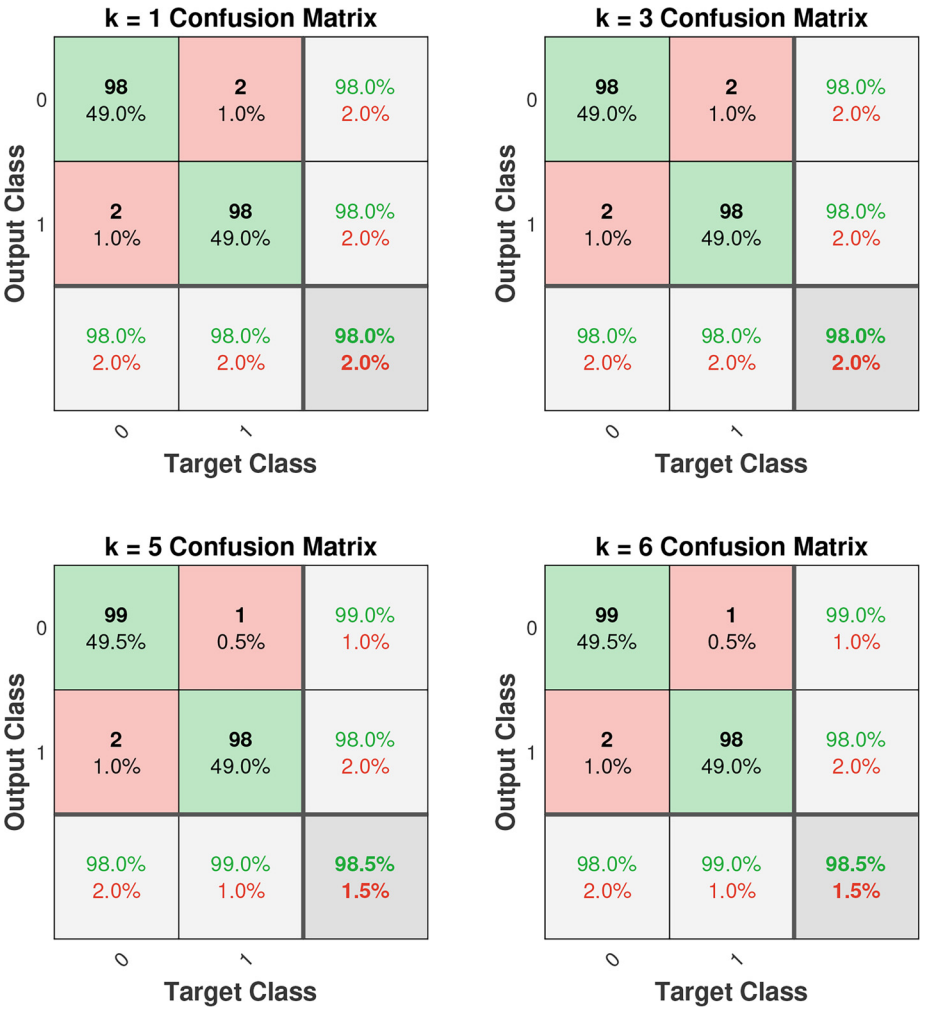


**Figure 7.**
Confusion matrices in the second scenario, when both training and testing are made with targets at varying distance

**Notes:** *Class 0* stands for the square, whereas *Class 1* stands for the circular plate. The numbers of correctly classified targets are in the main diagonal (green) whereas the off-diagonal elements are incorrectly classified (red)
**Source:** Authors' own work

the "Triangle+Circle" targets are correctly classified, and the right side of the column displays the percentages of the in/correctly classified observations for each predicted classes of ours, such as 74% of the "Circle+Rectangle" targets are correctly classified with 26% error rate.

## 5. Conclusion

Radars operating in the mmWave band are essential parts of, among others, DAS. In this paper, some challenges are exposed in two related domains. First, we investigate the

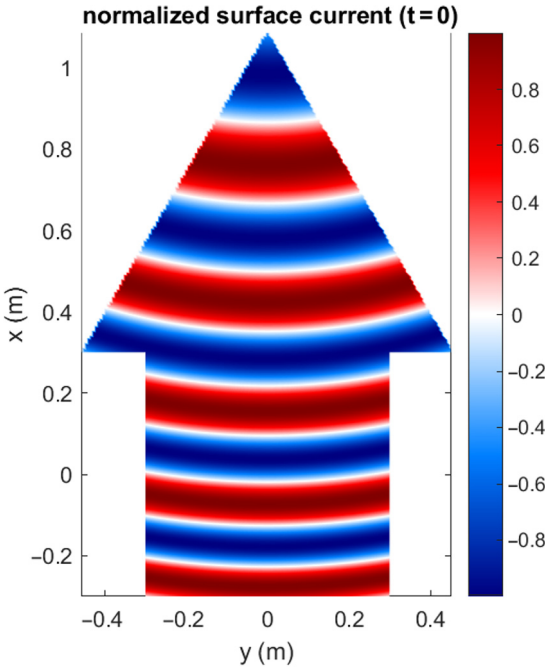


**Source:** Authors' own work

**Figure 8.**
A complex target consisting of a triangle and a square plate, and the distribution of the surface current density at a certain position of the antenna

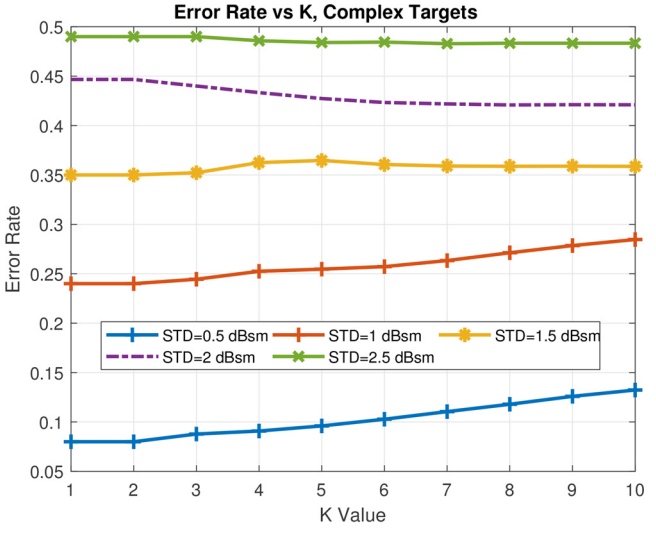


**Source:** Authors' own work

**Figure 9.**
Error rate vs $K$ for complex targets, at different values of the noise STD

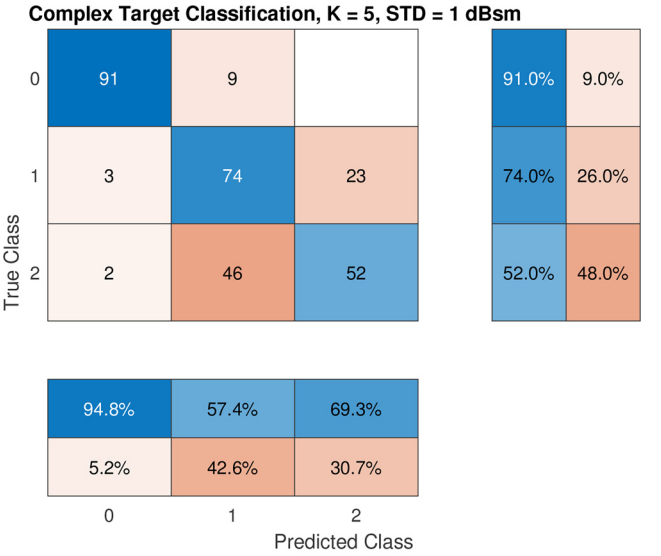


**Figure 10.**
Confusion matrix for complex targets (classes are in the order of "Triangle+Circle," "Circle+Rectangle" and "Triangle + Rectangle," respectively)

**Source:** Authors' own work

modeling of the electromagnetic scattering at such wavelengths, then we propose a post-processing method of radar echos for the solution of a target classification problem.

As targets are typically much larger than the wavelength, we apply the PO approximation to calculate the scattered field. Furthermore, targets are typically in the near-field of the radar's antenna. Therefore, the classical definition of the RCS cannot be used; we apply the near-field RCS instead.

The near-field RCS shows a very strong sensitivity to the incident angle. We stress that despite the deterministic physical model of the RCS, it is reasonable to consider the RCS as a random variable. Hence, we model the incident angle $\vartheta$ as a random variable with small variance, and we calculate the RCS repeatedly for several realizations of $\vartheta$. Then, we calculate a histogram from the RCS samples, and this histogram is considered as a feature of the target.

We propose a $K$-NN method for target classification based on the RCS histograms, where we use the L1 norm of the difference of histograms as a metric. In the examples, we chose targets that are conducting plates of different shapes, which is considered as a simple model of sensing traffic road signs by a DAS radar.

We present a set of benchmark examples to demonstrate the performance of the classification algorithm. The training and testing histograms are chosen in various ways, furthermore, we apply additive noise on the synthetic data to test the robustness of the algorithm. We show that the method is able to classify targets of different shapes, yet the error rate depends on the number of classes and on the strength of the noise that corrupts the data.

As a future work, we will study different metrics of the histograms, and we will introduce more complex targets, with a higher degrees of freedom, e.g. the area will also vary. More sophisticated classifiers, e.g. deep neural networks, will also be tested. Furthermore, we plan to collect measured data to reveal how our current model should be further refined.

## References

Bowman, J.J., Senior, T.B.A. and Uslenghi, P.L.E. (1969), *Electromagnetic and Acoustic Scattering by Simple Shapes*, Hemisphere Publishing Corp, London.

Cai, X., Giallorenzo, M. and Sarabandi, K. (2021), "Machine Learning-based target classification for MMW radar in autonomous driving", *IEEE Transactions on Intelligent Vehicles*, Vol. 6. pp. 678-689.

Devroye, L., Gÿorfi, L. and Lugosi, G. (1996), *A Probabilistic Theory of Pattern Recognition*, Springer, Cham.

Dudani, S.A. (1976), "The distance-weighted k-nearest-neighbor rule", *IEEE Transactions on Systems, Man, and Cybernetics*, Vol. SMC-6 No. 4, pp. 325-327.

Elfrgani, A. and Reddy, C.J. (2019), "Near-Field RCS for automotive radar applications", *2019 International Workshop on Antenna Technology (iWAT)*, pp. 217-220.

Gupta, S., Rai, P.K., Kumar, A., Yalavarthy, P.K. and Cenkeramaddi, L.R. (2021), "Target classification by mmWave FMCW radars using machine learning on range-angle images", *IEEE Sensors Journal*, Vol. 21 No. 18, pp. 19993-20001.

Kim, B.-S., Jin, Y., Lee, J. and Kim, S. (2022), "FMCW radar estimation algorithm with high resolution and low complexity based on reduced search area", *Sensors*, Vol. 22 No. 3, p. 1202.

Kosuge, A., Suehiro, S., Hamada, M. and Kuroda, T. (2022), "mmWave-YOLO: a mmWave imaging radar-based real-time multiclass object recognition system for ADAS applications", *IEEE Transactions on Instrumentation and Measurement*, Vol. 71, pp. 1-10.

Kouyoumjian, R.G. (1965), "Asymptotic highfrequency methods", *Proceedings of the IEEE*, Vol. 53 No. 8, pp. 864-876.

Patel, K., Rambach, K., Visentin, T., Rusev, D., Pfeiffer, M. and Yang, B. (2019), "Deep learning-based object classification on automotive radar spectra", *2019 IEEE Radar Conference (RadarConf)*, pp. 1-6.

Pouliguen, P., Damiens, J.F., Hemon, R. and Saillard, J. (2006), "RCS computation in near field", *DAYS on DIFFRACTION 2006*, pp. 252-265.

Skolnik, M.I. (1990), *Radar Handbook*, 2nd ed., McGraw Hill, New York, NY.

Swerling, P. (1960), "Probability of detection for fluctuating targets", *IEEE Transactions on Information Theory*, Vol. 6 No. 2, pp. 269-308.

Taylor, J.M. and Terzuoli, A.J. (1997), "On the concept of near field radar cross section", *IEEE Antennas and Propagation Society International Symposium 1997. Digest*, Vol. 2, pp. 1172-1175.

Vaila, M., Jylhä, J., Väisänen, V., Perälä, H., Visa, A., Harju, M. and Virtanen, K. (2017), "A RCS model of complex targets for radar performance prediction", *2017 IEEE Radar Conference (RadarConf)*, pp. 430-435.

Vladyslav, K. and Maxim, L. (2016), "Statistical RCS processing", *2016 II International Young Scientists Forum on Applied Physics and Engineering (YSF)*, pp. 175-178.

**Corresponding author**
Sándor Bilicz can be contacted at: bilicz.sandor@vik.bme.hu